PAPER

Optimizing the magnetic properties of hard and soft materials for producing exchange spring permanent magnets

View the article online for updates and enhancements.

IOP **ebooks**™

Bringing together innovative digital publishing with leading authors from the global scientific community.

Start exploring the collection−download the first chapter of every title for free.

Optimizing the magnetic properties of hard and soft materials for producing exchange spring permanent magnets

Michele Petrecca[1,2] , **Beatrice Muzzi**[3] , **Stefano Maria Oliveri**[1], **Martin Albino**[1,4] , **Nader Yaacoub**[5], **Davide Peddis**[6] , **César de Julián Fernández**[7] , **Claudia Innocenti**[1,2] **and Claudio Sangregorio**[1,2]

[1] Department of Chemistry 'U. Schiff', University of Florence and INSTM, I-50019 Sesto Fiorentino (FI), Italy
[2] ICCOM—CNR, I-50019 Sesto Fiorentino (FI), Italy
[3] Department of Biotechnology, Chemistry and Pharmacy, University of Siena 1240, I-53100 Siena, Italy
[4] Department of Industrial Engineering, University of Florence, I-50139 Firenze, Italy
[5] IMMM, Université du Mans, CNRS UMR-6283, Avenue Olivier Messiaen, Le Mans 72085, France
[6] Department of Chemistry and Industrial Chemistry (DCIC), University of Genova, I-16146 Genova, Italy
[7] IMEM—CNR, I-43124 Parma, Italy

E-mail: martin.albino@hotmail.it and csangregorio@iccom.cnr.it

Abstract

The exploitation of the exchange coupling between hard and soft magnetic materials has been proposed for enhancing the magnetic performances of rare-earth free permanent magnets, with the aim of extending their use to all applications where moderate energy product ($35–100$ kJ m^{-3}) is required. Strontium hexaferrite (SFO)/spinel ferrite composites seem particularly promising to achieve this target, although the conditions to maximize the effect while using techniques easily scalable to industrial production have not yet been identified. Within this framework, the optimization of the structural, chemical, and magnetic properties of the two moieties before the coupling procedure is crucial to enhance the energy product of the final composite. Here we report the syntheses of both nanometric SFO with high coercivity (ca. 525 kA m^{-1}) and quasi-bulk saturation magnetization (68 Am^2 kg^{-1}) and a series of nanosized zinc-doped ferrite ($Zn_xFe_{3-x}O_4$, $0.0 \leqslant x \leqslant 0.4$) through cheap, easily scalable and eco-friendly approaches. The structural and chemical stability of the two magnetic phases as a function of temperature were investigated up to $1100\,^\circ$C, with the aim of finding the best compromise between preservation of the nanometric scale and magnetic properties. A very high-magnetization (106 Am^2 kg^{-1}) ferrite was obtained by annealing $Zn_{0.3}Fe_{2.7}O_4$ nanopowder at the highest investigated temperature. A preliminary attempt at coupling the two phases, starting from a mixture of the nanopowders, was performed through a classic annealing process in the temperature range $500\,^\circ$C–$1100\,^\circ$C. The adopted procedure allowed for obtaining an exchange coupled composite at $1100\,^\circ$C where the two phases are intimately and homogeneously mixed, with micrometric (0.3–$5\ \mu$m) and nanometric (up to 50 nm) spinel ferrite particles. Despite these promising results, no enhancement of the energy product was found, highlighting the need for further experimental efforts to improve the coupling procedure.

1. Introduction

Permanent magnets (PMs) are key elements of contemporary technology and can be found in a large number of devices operating in a huge variety of fields, including electronic, energy, automotive and data storage [1–4]. The applications of a PM are determined by the magnetic energy density that can be stored in the material per unit volume, which is described by the maximum energy product, BH_{max}, where B is the magnetic induction and is given by $B = \mu_0(H + M)$, μ_0 being the vacuum permeability ($\mu_0 = 4\pi \times 10^{-7}$ Hm^{-1}), H the applied magnetic field and M the magnetization of the material. In other words, BH is the combination of the operative flux density (the magnetic induction, in working condition) and the magneto-motive force (the resistance of the magnet to demagnetization). High-performance rare-earth (RE)-based PMs (RE-PMs) are used in all applications where high BH_{max} values are needed. In RE-PMs, the high anisotropy of RE combined with the high magnetic moment of the transition metals leads to BH_{max} values about 5–10 times higher (e.g. from 100 kJ m^{-3} to over 400 kJ m^{-3} for NdFeB) than in other PMs, such as strontium or barium hexaferrite (35–45 kJ m^{-3}) or alnico alloys (45–80 kJ m^{-3}) [4]. However, despite their very high performances, RE-PMs present important drawbacks, such as high costs (from hundreds to tens of thousands of euros per kilogram), high supply risk and serious environmental impact (acidic wastewater and radioactive residues generated in the refinement process) [5, 6]. Nevertheless, currently most technological applications use RE-PMs, although a significant number of them (mainly in the automotive and energy industries) require magnets with only a moderate energy product within the range of 35–100 kJ m^{-3}. An increase in the energy product of standard ferrites would thus allow the replacement of RE-PMs in all those applications requiring low/medium-performing PMs, reducing the dependence on these critical materials.

Among the different approaches proposed so far to maximize the BH_{max} of RE-free PMs, a lot of attention has been paid towards nanostructured hybrid materials based on the coupling of a hard and a soft magnetic material. Hard/soft composites are expected to benefit from the properties of both components. In fact, the exchange interaction between the spins at the interface may allow a significant enhancement of the remanence of the hybrid nanocomposite with only a moderate decrease in the coercive field [7, 8]. Theoretical models for bilayer 2D systems [7] predict that the two magnetic phases are coupled when the size of the soft component is lower than 2–3 times the exchange length of the hard phase [9, 10]. The extension of this theory to nanoparticles has not been demonstrated yet. Interestingly, a recent investigation by Quesada *et al* [11] on the magnetic properties of core@shell CoFe$_2$O$_4$@CoFe nanoparticles, where the size of both phases is above the theoretical exchange length and below the single-domain size, suggested that even a weak coupling could give rise to single-step loops and enhanced BH_{max}.

Several attempts to fabricate exchange-coupled magnetic materials with improved BH_{max} have been reported in the literature, using different building blocks and production techniques [12–18]. Among the hard materials investigated so far, strontium hexaferrite (SFO) has received large attention owing to its chemical stability, large availability, low production cost and good magnetic properties (saturation magnetization $M_S = 70$–72 Am^2 kg^{-1}, coercivity $H_C = 400$ kA m^{-1} and BH_{max} close to 40 kJ m^{-3}), characteristics that make it a leading candidate in the PM market. Large efforts have been spent on increasing the BH_{max} of SFO by combination with hard or soft spinel cubic ferrite (MFe$_2$O$_4$ M=Co, Fe, Mn) or metal alloys (FeCo) [19–25]. In view of the possible production at the industrial scale, the use of metal oxides is particularly promising due to their stability against corrosion and mechanical processing. In principle, the fundamental requisite of a large enough magnetization to enhance the remanence of the composite is satisfied by several spinel ferrites, such as magnetite, nickel–zinc-doped magnetite or zinc ferrite. Nevertheless, to the best of our knowledge, no cubic ferrites with M_S larger than 95 Am^2 kg^{-1} have been explored for this purpose to date [15, 20, 22, 23, 26, 27]. An interesting example of combination of SFO with a metal oxide was reported by Jenus *et al* [26]. The authors showed that the application of the spark plasma sintering technique to a mixture of SFO and cobalt ferrite magnetic nanoparticles (MNPs) prepared by hydrothermal synthesis led to an increase in BH_{max} of ca. 20%, up to 26.1 kJ m^{-3} with respect to pure SFO. However, the magnetic properties of the starting nanometric powders ($H_C = 117$ kA m^{-1} and $M_S = 27$ Am^2 kg^{-1} for SFO and $M_S = 78$ Am^2 kg^{-1} for CoFe$_2$O$_4$) were lower than those of the corresponding bulk materials.

Despite the many attempts, the target of a significant increase in the energy product of SFO above 40 kJ m^{-3} has not yet been achieved. To reach this goal, careful control of the quality of the starting nanopowders can be beneficial. On the other hand, it should be taken into account that the sintering–annealing process can also drastically affect the magnetic properties of both moieties, due to the increase in crystal size, the displacement of ions among the cavity within the oxide lattice, and the chemical reactivity [28–32]. Therefore, the understanding of the evolution of the properties of each single component with temperature is also essential to design the best exchange-coupled materials.

J. Phys. D: Appl. Phys. **54** (2021) 134003

M Petrecca *et al*

The work here presents progress within this context, as it addresses the synthesis of a hard ($SrFe_{12}O_{19}$) and a soft ($Zn_xFe_{3-x}O_4$, $x < 0.5$) nanometric component with optimized magnetic properties to be coupled by an annealing procedure, and the investigation of their thermal stability. The selected synthetic approaches are cheap, eco-friendly, and easily scalable to industrial production. The parameters of these syntheses are tuned to maximize the coercivity and the saturation magnetization of SFO nanoparticles, and to obtain a soft moiety with M_S above 100–105 Am^2 kg^{-1}.

2. Experimental

2.1. Chemicals and materials

All chemicals were used without any further purification. Zinc chloride ($ZnCl_2 \geqslant 98\%$), ferric chloride hexahydrate ($FeCl_3 \cdot 6H_2O$, 98%), ferrous chloride tetrahydrate ($FeCl_2 \cdot 4H_2O$, 98%), strontium chloride ($SrCl_2$, $\geqslant$99%), and sodium hydroxide (NaOH, $\geqslant$98%) were purchased from Aldrich Chemical Co, and absolute ethanol (EtOH) and acetone were purchased from Fluka.

2.2. $Zn_xFe_{3-x}O_4$ nanoparticle synthesis

Zinc-doped magnetite with variable composition, $Zn_xFe^{2+}_{(1-x)}Fe^{3+}_2O_4$ ($0 \leqslant x \leqslant 0.4$, $x = 0$, 0.1, 0.2, 0.3, 0.4), was synthesized by co-precipitation. The molar ratio of starting Zn^{2+} and Fe^{2+} chlorides was quantitatively adjusted according to the final desired stoichiometry (see table S1 in the supporting information (available online at stacks.iop.org/JPD/54/134003/mmedia) for details). A basic solution was prepared by dissolving 40 g of NaOH in 400 ml of demineralized water and, under N$_2$ flow and magnetic stirring, it was heated up to reflux. Meanwhile, the stoichiometric amounts of $ZnCl_2$ and $FeCl_2 \cdot 4H_2O$ and 13.5 g of $FeCl_3 \cdot 6H_2O$ were solubilized in 100 ml of N$_2$-purged demineralized water. This solution was quickly added dropwise to the basic one and the resulting black reaction mixture was kept at reflux for 2 h, under N$_2$ flow and magnetic stirring. Then, the black suspension was cooled down to room temperature and the black precipitate was collected using a PM. The MNPs were washed several times with water, ethanol and acetone and dried overnight at 80 °C. The resulting black powder (ca. 5.6 g with a yield of ca. 95%) was stored under inert atmosphere.

In the following, zinc-doped magnetite samples will be labeled as ZFO*xx*, where *xx* denotes the zinc content (i.e. $x = 0.1$ corresponds to *xx* = 01).

2.3. $SrFe_{12}O_{19}$ nanoparticle synthesis

$SrFe_{12}O_{19}$ nanoparticles (SFO) were synthesized through a low-temperature solid-state method followed by calcination, according to a procedure slightly modified from [33]. In a typical synthesis, 1.32 g of $SrCl_2$ and 13.52 g of $FeCl_3 \cdot 6H_2O$ were crushed, mixed, and added to 9.00 g of finely crushed NaOH in a mortar, causing the resulting brownish mud to heat

up. The mixture was mixed for 5 min and then washed on a Büchner funnel several times with demineralized water, until a pH value of 8 was reached. The resulting mud was dried at 80 °C overnight, obtaining ca. 4.5 g of orange-brownish powder. The as-obtained amorphous powder was calcinated in a furnace at 775 °C for 3 h, obtaining ca. 4.3 g (yield ca. 97%) of a dark brown M-ferrite powder.

2.4. Hard/soft composite synthesis

Soft–hard hybrid systems were obtained by mixing SFO/ZFO03 nanometric powders (90/10 weight ratio) in a mortar, adding a few drops of acetone to homogenize the mixture. The resulting powder was annealed in a tubular furnace under N$_2$ flow at different temperatures (500 °C, 700 °C, 900 °C and 1100 °C) for 2 h. The heating rate was 10 °C min^{-1} up to the target temperature; the cooling process was controlled down to 700 °C with a rate of 5 °C min^{-1}, while for lower temperature the furnace was left to cool down freely. In the following, the obtained samples will be labeled as MIX-*xxx*C where *xxx* is the annealing temperature, while the mixed powder not exposed to the thermal process will be simply labeled as MIX.

2.5. Characterization techniques

Transmission electron microscopy (TEM, CM12 Philips equipped with a LaB$_6$ filament operating at 100 kV) was employed to determine the morphology and size distribution of the MNPs. The mean diameter and the MNP size distribution for each sample were obtained by statistical analysis over more than 100 MNPs, using ImageJ software. Scanning electron microscopy (SEM, HITACHI S2300 equipped with a tungsten filament as the electron beam source, acquiring images at 20 keV) was used to determine the size and morphology of the annealed samples. Energy-dispersive x-ray (EDX) analysis was carried out on a TESCAN GAIA 3 SEM microscope equipped with an EDAX Octane Elect Super EDX detector. Powder x-ray diffraction (XRD) patterns were recorded using a Bruker New D8 ADVANCE ECO diffractometer equipped with a Cu Kα (1.5406 Å) radiation source and operating in θ–2θ Bragg–Brentano geometry at 40 kV and 40 mA. Lattice parameter a and mean crystallite diameter d_{XRD} were evaluated by TOPAS software (Bruker) using the method of fundamental parameter approach. The measurements were carried out in the angular range 25°–70°, with a step size of 0.03° and collection time of 0.5 s. The magnetic properties were investigated using a Quantum Design MPMS superconducting quantum interference device and physical property measurement system vibrating sample magnetometers on randomly oriented pressed powder pellets or on powders dispersed in a low-melting wax. The stoichiometry of the MNPs was checked by Inductively coupled plasma atomic emission spectroscopy (ICP-AES) using a Varian 720-ES. ^{57}Fe Mössbauer spectra were recorded using a ^{57}Co/Rh γ-ray source mounted on an electromagnetic transducer with a triangular velocity form. The hyperfine structure was modeled by a least-squares fitting procedure involving Zeeman sextets and quadrupolar doublets
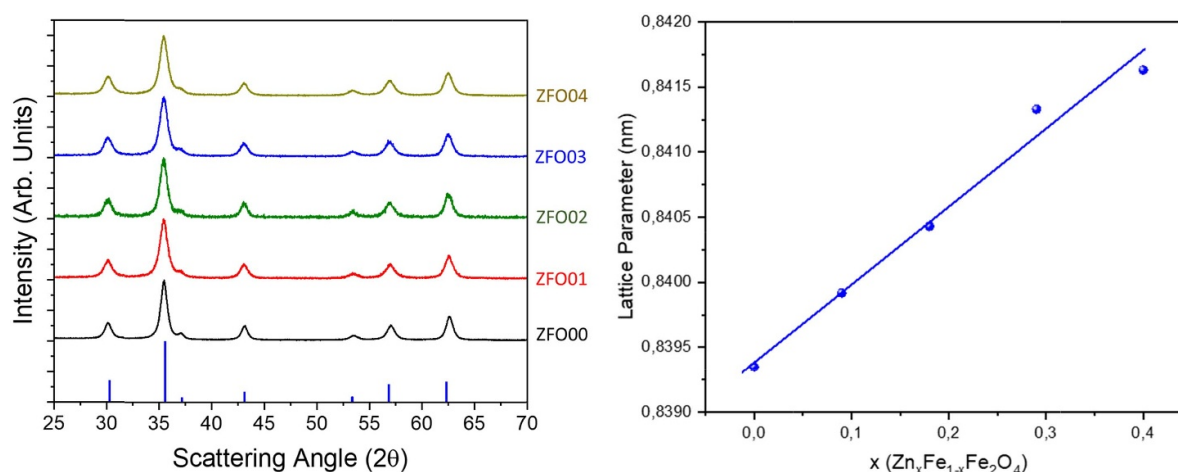
Figure 1. Left panel: XRD patterns of the Zn-doped magnetite samples. The blue reference bars correspond to the magnetite pattern (JCPDF: 88-0315). Right panel: lattice parameter *a* dependence on the Zn content *x* (error < 0.001). The straight line is a guide for the eyes.

composed of Lorentzian lines using Mosfit software. The isomer shift values are referred to as that of α-Fe at 300 K.

3. Results and discussion

3.1. Synthesis of the soft phase

Spinel ferrites AFe_2O_4 are an extremely versatile platform to develop the soft phase, as they present high chemical and physical stability and a high M_S value. Their crystalline structure can be described by a ccp oxide ion packing which defines tetrahedral (Td, round bracket) and octahedral (Oh, square bracket) cavities occupied by different divalent ions (A = Fe, Mg, Co, Mn, Zn, etc) and Fe^{3+} ions. Fine tuning of the magnetic properties can thus be obtained by simply replacing, either completely or partially, the metal ions or by modifying the inversion degree without affecting the crystal structure. Typically, a strategy to increase M_S is the partial replacement of Fe^{2+} ions with diamagnetic Zn^{2+} ions. Since Zn^{2+} ions preferentially occupy Td sites in the inverse spinel structure, their introduction partially removes the antiferromagnetic coupling between Fe^{3+} in Td and Oh sites, making the Td and Oh sublattices more unbalanced. However, this mechanism holds up until the Zn^{2+} substitution reaches ca. half of the total number of divalent ions [34]. For a higher percentage, M_S starts decreasing due to the weakening of the magnetic exchange between Td and Oh sites, which induces destabilization of the ferrimagnetic order and local canting of the spins in the Oh sites [35–37].

To investigate the effect of the Zn substitution on the magnetic properties of the doped ferrite nanoparticles and to identify the stoichiometry that maximizes the M_S of the material, a family of samples with variable composition, $Zn_xFe^{2+}_{(1-x)}Fe^{3+}_2O_4$, x = 0, 0.1, 0.2, 0.3, 0.4, was prepared. The effective stoichiometries of the synthesized samples, checked by ICP-AES analysis, confirmed the amount of Zn and Fe in the spinel lattice was, within the experimental error, almost identical to that set in the synthesis (figure S1

of supporting information). In the XRD patterns of the as-synthesized samples (figure 1, left panel), all the reflexes could be indexed to the cubic spinel structure $Fd\bar{3}m$ and no other peaks were observed, confirming that the introduction of Zn does not induce the formation of secondary phases.

The crystal sizes and lattice parameters of the series were obtained by the Pawley method [38]. For all the samples, the crystal size was found to be ca. 10 nm, while an increase in the lattice parameter was observed from 0.8393(1) nm for ZFO00 to 0.8416(1) nm for ZFO04. As reported in the literature on the corresponding bulk and nanosized materials [34, 39], the increase in the lattice parameter with Zn content (figure 1, right panel, and table 1) confirms that the Zn^{2+} ions are effectively incorporated in the ferrite lattice. In fact, the theoretical model proposed by O'Neill and Navrotsky [40] predicts that a linear increase in the lattice parameter is observed only if Zn^{2+} ions replace Fe^{3+} in Td cavities. In our case, the match between experimental and theoretical data suggests that the zinc ions occupy the Td sites of the lattice. TEM images and corresponding statistical analyses are reported in figure S2 in the supporting information and show that all the samples consist of nanoparticles of ca. 10 nm diameter. The good agreement between the average MNP diameter obtained from TEM and the crystallite size from XRD measurements (table 1) suggests that all samples are composed of single-crystal MNPs. To evaluate the effect of the Zn substitution on the magnetic properties of ZFO MNPs, the field dependence of the magnetization, $M(H)$, was investigated at 300 K. All the samples are superparamagnetic (i.e. zero coercivity, zero remanence within experimental error) at 300 K. The $M(H)$ curves reach saturation at the highest measured fields, so that the saturation magnetization values, M_S, can be estimated as $M_S = M(5\ T)$ (table 1).

The M_S for magnetite MNPs (ZFO00) ($M_S = 69\ Am^2\ kg^{-1}$) is lower than that of the bulk (92 $Am^2\ kg^{-1}$ at 300 K [41]), but comparable with that reported in the literature for magnetite MNPs prepared by co-precipitation [42]. This decrease can be ascribed to structural and/or magnetic disorder typical of MNPs prepared by this method. As mentioned above, in

J. Phys. D: Appl. Phys. **54** (2021) 134003

M Petrecca *et al*

Table 1. Chemical, structural and magnetic properties of ZFO*xx* MNPs. *x*: Zn content obtained from ICP analysis; d_{XRD}, *a*: crystallite mean size and lattice parameter obtained from XRD data analysis (errors on the least significant digit are reported in brackets); d_{TEM}: MNP average diameter and standard deviation obtained from statistical analysis of the TEM images; M_S: saturation magnetization estimated as $M_S = M(5\,T)$.

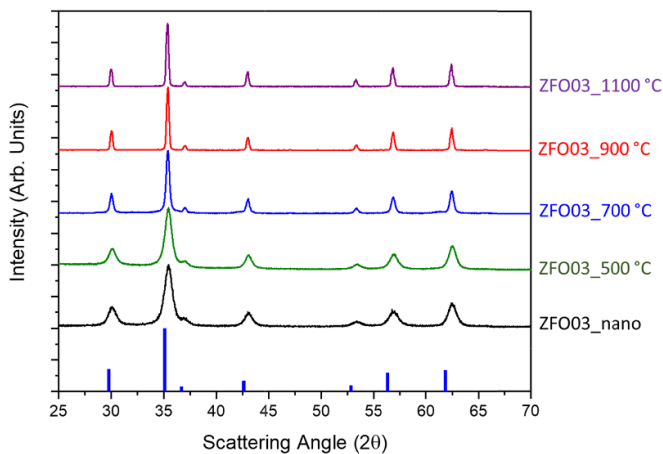| Sample	*x* ICP ($Zn_xFe_{(3-x)}O_4$)	d_{XRD} (nm)	*A* (nm)	d_{TEM} (nm)	M_S (A m^2 kg^{-1})
ZFO00	0	10(1)	0.8393(5)	10.7 ± 2.9	69(1)
ZFO01	0.09	9(1)	0.8399(2)	9.5 ± 2.3	75(1)
ZFO02	0.18	10(1)	0.8404(3)	10.8 ± 2.3	79(1)
ZFO03	0.27	9(1)	0.8413(3)	9.9 ± 2.2	77(1)
ZFO04	0.4	9(1)	0.8416(3)	9.5 ± 2.4	76(1)

Figure 2. XRD patterns of ZFO03 powder annealed at different temperatures (500 °C, 700 °C, 900 °C and 1100 °C) for 2 h. The bottom blue reference is the magnetite one (JCPDF: 88-0315).

bulk Zn-ferrites, the M_S follows a non-linear trend with the progressive introduction of diamagnetic Zn ions in the lattice reaching a maximum of $x = 0.5$ [37]. A non-monotonic behavior, but with a maximum shifted to $x = 0.2$, can be observed for our samples. Comparable results, both in terms of M_S and of correlation between zinc doping and M_S, were obtained by Liu *et al*, who reported a maximum $M_S = 81$ Am^2 kg^{-1} for $x = 0.2$ for Zn-ferrite nanoparticles synthesized through a similar procedure [43]. The shift with respect to the bulk can be ascribed to the weakening of magnetic exchange coupling due to the increase in spin disorder occurring at the nanoscale [44].

On the basis of these results, with the aim of increasing the magnetic order of the MNPs, the ZFO*xx* series underwent an annealing process into a tubular furnace under inert atmosphere (N_2), at different annealing temperatures in the range 500 °C–1100 °C with an increment of 200 °C and dwelling time of 2 h at the target temperature. Since the obtained results, reported in table S2 in the supporting information, were similar for all the samples of the series, for the sake of clarity, only sample ZFO03 will be discussed in detail in the following. XRD patterns as a function of annealing temperature are reported in figure 2.

It is important to note that in all the recorded XRD patterns only the cubic spinel structure appears (figure 2). This

result is particularly relevant as it confirms the effectiveness of the chosen thermal treatment conditions. Numerous studies indeed indicate that the spinel phase is thermally unstable and can decompose at high temperature, leading to the formation of secondary crystallographic phases like wüstite (FeO), hematite (α-Fe_2O_3) and zinc oxide (ZnO) [45–47]. The lattice parameter of the thermally treated sample does not change with temperature within the error of the fitting process, while the crystallite diameter remains at ca. 10 nm for powders treated at 500 °C and then increases above the resolution of the instrument (instrumental broadening) when the annealing temperature exceeds 900 °C. To observe the morphology and grain size of the samples exposed to the thermal treatment, SEM images are also acquired (figure S3, supporting information). The grain size increases as a function of heating temperature: at 500 °C and 700 °C the grains maintain a nanometric size, at 900 °C large aggregates of (sub)micrometric particles appear, while at 1100 °C partially sintered micrometric grains are formed. All these observations are consistent with the XRD peak linewidth evolution. The magnetic hyperfine structure (MHS) extracted from Mossbauer spectra recorded at 300 K (figure S4, supporting information) can be described using two contributions related to the trivalent iron in the tetrahedral sites (Fe^{3+}Td) and to a mix of divalent and trivalent iron in the octahedral sites ($Fe^{2.5+}$Oh). The MHS exhibits some similarities with that of a stoichiometric magnetite, showing two magnetic sextets, one attributed to the Fe^{3+} ions located in the Td sites and the other one to $Fe^{2.5+}$ ions with an intermediate valency state in the Oh sites. This suggests that thermal treatments do not induce a significant oxidation process of Fe^{2+}. It has to be noted that the stability of Fe^{2+} ions and the lack of segregation of other iron oxides, such as hematite, are not easy tasks to be realized. In our case, we attributed this result to the controlled heating ramp and the use of inert atmosphere. The M_S dependence on Zn content as a function of thermal treatment is shown in figure 3 (values are reported in table S3 in supporting information). A marked increase in M_S with annealing temperature is observed for all the samples of the series. The non-linear trend of M_S with the progressive introduction of diamagnetic Zn^{2+} ions, observed for the as-prepared nanopowders, is preserved after the thermal treatment, but the maximum M_S shifts to $x = 0.3$ for higher annealing temperatures. This behavior agrees with the progressive minimization of spin disorder associated with the growth of the grain up to the micrometric scale.
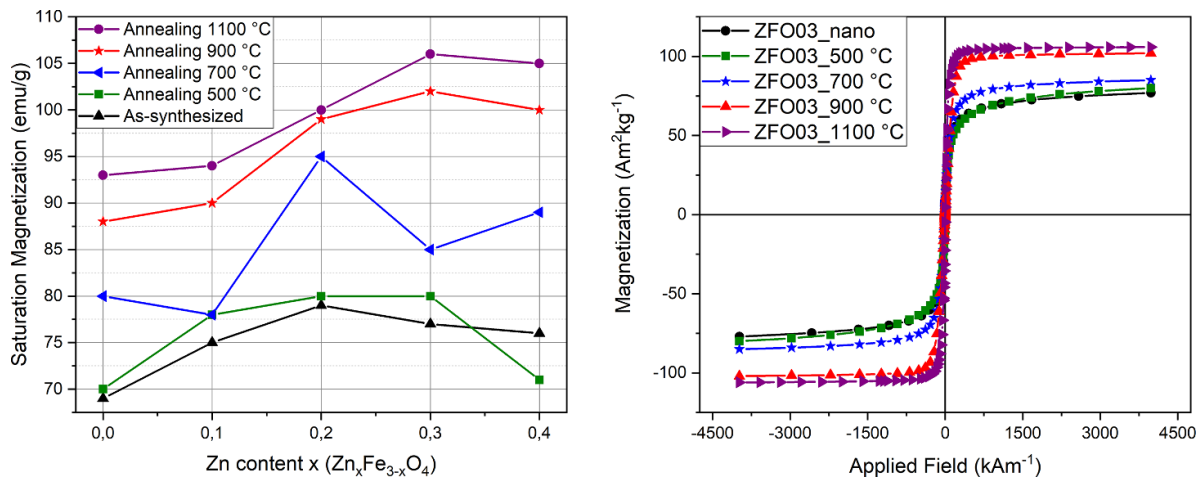
J. Phys. D: Appl. Phys. **54** (2021) 134003

M Petrecca *et al*

Figure 3. Left: saturation magnetization evolution as a function of Zn content *x* for samples annealed at different temperatures; right: hysteresis loop evolution as a function of annealing temperature for $Zn_{0.3}Fe_{2.7}O_4$; the loops were recorded at room temperature.

The most promising sample for the purpose of this work is ZFO03, which once annealed at 1100 °C for 2 h reached $M_S = 106 \, \text{Am}^2 \, \text{kg}^{-1}$. This value is in accordance with the ones reported in the literature for MNPs with the same composition and crystal size above 100 nm, obtained through the less cost-effective method of thermal decomposition [48].

3.2. Synthesis of the hard phase

Micrometric $SrFe_{12}O_{19}$ is a commercial material with good magnetic properties (non-oriented grains display a BH_{max} of ca. 8 kJ m^{-3}) [34, 49, 50]. This material was deeply investigated to be employed as a single component for the production of PMs, for which its remanence, M_R and BH_{max} have been strongly improved through technological methodologies (up to 72 Am^2 kg^{-1} and ca. 40 kJ m^{-3}, respectively). In order to realize an efficient building block for exchange-coupled PM production, the synthesis of nanometric $SrFe_{12}O_{19}$ powder with a high surface area and similar or better magnetic properties than commercial ones is required.

In this work, SFO MNPs were synthesized through a solid-state method followed by a calcination procedure [33]. TEM images of the SFO sample are shown in figures 4 (left) and S5 in the supporting information. They depict the presence of MNPs with a platelet morphology and an average diameter of ca. 100 nm. In the XRD pattern, shown in figure 4 (right), all the peaks of the M-hexaferrite structure belonging to the $P6_3/mmc$ space group are recognized.

From Pawley refinement of the XRD pattern, the crystallite size was evaluated to be 100(14) nm, while the lattice parameters *a* and *c* were 0.5887(1) nm and 2.3064(1) nm. These values are in good agreement with those reported in the literature for the M-type SFO [51–53]. The magnetic properties were evaluated by recording the field dependence of magnetization at 300 K. From the hysteresis loop reported in figure 5, $M_S = 68 \, \text{Am}^2 \, \text{kg}^{-1}$, $M_R = 34 \, \text{Am}^2 \, \text{kg}^{-1}$ ($M_R/M_S = 0.5$) and $H_C = 525 \, \text{kA m}^{-1}$ were estimated. The M_S value is comparable with the bulk one [53], while H_C is very high and, importantly, is larger than that of commercial powders.

Next, we investigated the evolution of the magnetic properties of the SFO powder as a function of temperature. To this end, the SFO MNPs were treated in a tubular furnace at 500 °C, 700 °C, 900 °C and 1100 °C under inert atmosphere (N$_2$) for 2 h. XRD patterns (figure 6) revealed the structural stability of the SFO, since no other crystallographic phases were found, nor was variation of the lattice parameters *a* or *c* observed (table 2). Conversely, the grain size remained constant up to 700 °C and then started to grow, reaching ca. 370 nm for $T_{ann} = 1100$ °C (table 2).

M_S and M_R remained almost constant in the series, apart from a slight increase in M_S (72 Am^2 kg^{-1}) for SFO_1100 °C, mostly due to the larger size of the grains and the corresponding reduction of finite-size effects. As crystal size increased, the coercivity decreased to ca. 45% of the pristine nano-powder for SFO_1100 °C. This behavior reflects the change of magnetization reversal mechanism from coherent rotation typical of the single-domain state to nucleation and domain wall motion characteristic of particles with multi-domain spin configuration, associated with the grain growth. The critical diameters for the single- to multi-domain spin configuration transition for SFO are commonly reported to be in the 0.5–1.5 μm range [54–56], which is higher than the grain size explored in this work. However, several reports demonstrate that above 100 nm non-uniform reversal modes or the coexistence of single- and multi-domain states may occur [57], producing a decrease in the coercive field.

These data suggest that at 900 °C the crystal phase is stable, the grain size is still in the nanometric range and good magnetic properties are preserved. This temperature is thus a good compromise between the thermal energy, which in the following should promote coupling between the hard and soft magnetic phases, and the preservation of sub-micrometric grains and high coercive field.

3.3. Exchange coupled hard/soft $SrFe_{12}O_{19}/Zn_{0.3}Fe_{2.7}O_4$ composite

After the two best building blocks were identified, a preliminary study was carried out through a standard annealing
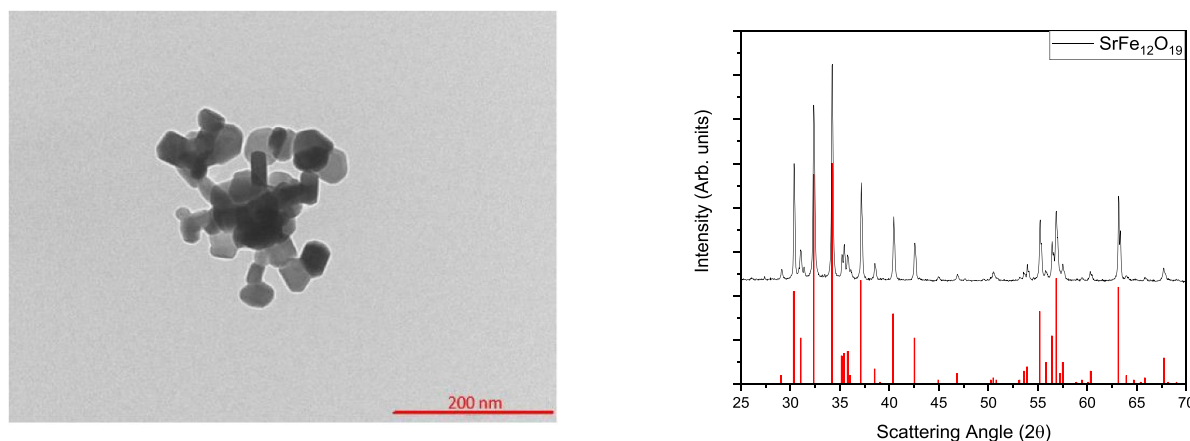
Figure 4. (Left) Representative TEM image of the SFO MNPs; (right) XRD pattern of the M-type hexaferrite phase obtained by solid-state synthesis. The red pattern at the bottom is the reference for strontium hexaferrite (JCPDF: 33-1340).
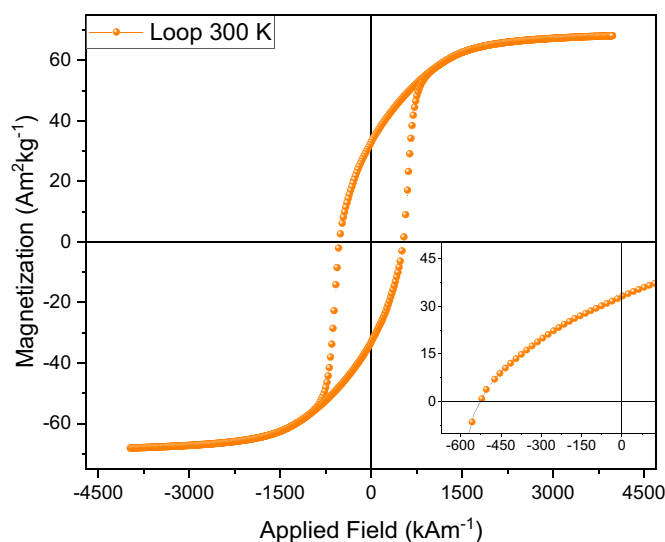

Figure 5. Magnetization as a function of the applied field recorded at 300 K. The inset shows the low-field region.

approach, to realize a hard/soft composite and to determine the experimental conditions needed to produce an exchange-coupled magnet. Thanks to the high saturation magnetization of the soft phase, the addition of a percentage as small as $10\%_{w/w}$ should allow an increase in M_S of SFO up to $75.4\,\mathrm{Am^2\,kg^{-1}}$ with only a small decrease in the total coercivity. Then, as a first attempt, hard/soft hybrid systems were prepared by mixing SFO/ZFO03 nanometric powders in a 90:10 weight ratio, and annealing at different temperatures (500 °C, 700 °C, 900 °C and 1100 °C) for 2 h. XRD patterns (figure 7) of the as-prepared and annealed samples showed the presence of both crystallographic phases in the expected 90:10 ratio, as quantified by Rietveld refinement. At 1100 °C, the soft phase can be better identified because of the narrowing of the two peaks at $\theta = 30.0$ and 62.4 (denoted by the * in figure 7) due to the increase in crystal size. EDX analysis on powders (supporting information, table S4) confirmed the stoichiometry of the composites matches the expected one. The lattice parameters

are reported in table 3 and showed that no structural modifications occurred during the annealing process. Therefore, we can conclude that no chemical reactions between the two powders occurred in the investigated temperature range. The stability of the SFO and spinel ferrite mixture upon calcination has been previously reported in the literature [19, 21, 23]. However, in these cases a calcination treatment was needed to fully crystallize the starting nanopowders. In our case, since the selected ZFO contains Fe^{2+}, calcination under oxygen would lead to oxidation of the ferrite and formation of crystallographic phases with lower M_S, such as maghemite or hematite. Thus, the thermal treatment was carried out in inert atmosphere, avoiding the occurrence of oxidation and/or phase segregation.

The variation in size of the SFO crystal domains, obtained by fitting of the XRD patterns, in the composites with the annealing temperature showed the same trend and the same values as found for the SFO alone: it remained almost constant up to 700 °C and then started growing, reaching 345(40) nm at 1100 °C. The crystal size of the soft phase in the composite also started to grow after 700 °C, reaching its largest value for the highest investigated temperature (50(10) nm for 1100 °C). However, this value is much lower than the one observed when annealing ZFO MNPs alone (at 1100 °C micrometric sizes were attained). This evidence suggests that the adopted procedure led to intimate mixing between the two magnetic phases, which allowed the soft grain to preserve the nanometric size.

To properly investigate the evolution of grain size with temperature, SEM images were acquired of the four composites (figure 8). In agreement with diffraction data, for the samples annealed at temperature up to 900 °C, the grain growth was very limited and submicrometric grains with size comparable with those obtained by fitting the XRD patterns were observed. Conversely, in MIX-1100 °C a larger size distribution of particles was observed, since agglomerated submicrometric particles coexist with polycrystalline grains of a few micrometres.

EDX analysis in SEM mode was carried out on MIX-1100 °C. The color mappings of strontium, iron, zinc,
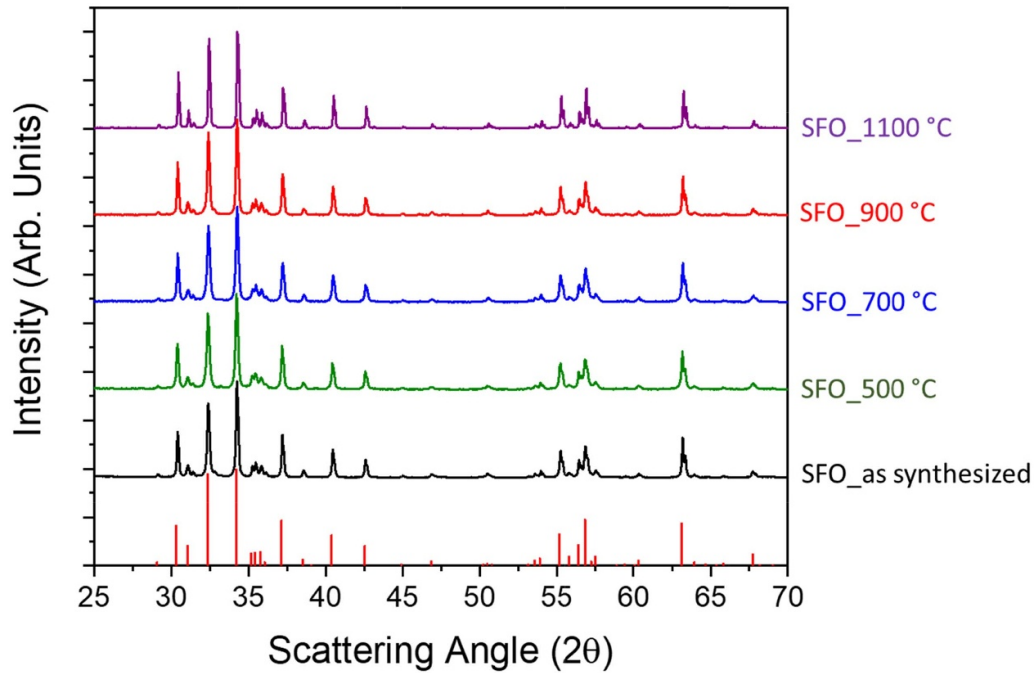
J. Phys. D: Appl. Phys. **54** (2021) 134003

M Petrecca *et al*

Figure 6. XRD patterns of the SFO powder annealed at different temperatures (500 °C, 700 °C, 900 °C and 1100 °C) for 2 h. The red bars correspond to the reference pattern of strontium hexaferrite (JCPDF: 33-1340).

Table 2. Structural and magnetic properties of SFO MNPs. d_{XRD}, a and c: crystallite mean size and lattice parameters obtained from XRD data analysis (errors on the least significant digit are reported in brackets); M_S: saturation magnetization estimated as $M_S = M(5\ \text{T})$; M_R: remnant magnetization; $R_\%$: reduced remnant magnetization $R_\% = M_R/M_S$; H_C: coercive field; BH_{max}: maximum energy product.

Sample	d_{XRD} (nm)	a (nm)	c (nm)	M_S (A m^2 kg^{-1})	M_R (A m^2 kg^{-1})	$R_\%$ (%)	H_C (kA m^{-1})	BH_{max} (kJ m^{-3})
As synthesized SFO	100(14)	0.5887(1)	2.3065(1)	68(1)	34(1)	50.0	525(2)	7.9(1)
SFO_500 °C	90(17)	0.5885(1)	2.3058(1)	68(1)	33(1)	50.0	427(2)	7.9(1)
SFO_700 °C	90(17)	0.5885(1)	2.3055(1)	68(1)	34(1)	50.0	431(2)	7.9(1)
SFO_900 °C	133(3)	0.5885(1)	2.3060(1)	69(1)	34(1)	49.3	381(2)	8.0(1)
SFO_1100 °C	370(20)	0.5886(1)	2.3062(1)	72(1)	34(1)	47.2	279(2)	7.6(1)

and oxygen are shown in figure 9. As expected, oxygen and iron were homogeneously distributed in the whole sample. Surprisingly, strontium and zinc also showed the same distribution. The absence of localized regions with higher abundance of zinc suggests that the growth of the ZFO nanoparticles is very limited and remains under the EDX resolution. In fact, combining XRD, SEM and EDX data, we can argue that the ZFO occurs in the composite as small, ca. 50 nm nanoparticles, homogeneously covering the surface of micrometer- and sub-micrometer-sized SFO particles. It is important to note that the grain sizes obtained for SFO match the single- to multi-domain threshold (0.5–1.5 μm), which corresponds to the size where a maximum of the coercivity occurs [54–56].

The field dependence of the magnetization (first magnetization curves and hysteresis loops) of the samples were recorded at room temperature (figure 1) on powders dispersed into a low melting wax, in order to avoid the preferential orientation of the nano-crystallites under the external field. To better highlight the presence of exchange spring behavior, the experimental hysteresis curves were compared with those

obtained by summing the hysteresis of the two independent phases, annealed at the same temperature, weighed by the same composition percentage of the MIX sample.

The calculated and experimental curves are almost superimposable up to 900 °C, with a difference in the saturation magnetization value between the two curves of max. 3% for the sample annealed at 700 °C. Thus, the magnetic coupling can be reasonably assumed to be null or negligible for this range of temperature. Conversely, the sample annealed at 1100 °C shows a different shape: the M_S of MIX-1100 °C is higher (82 Am^2 kg^{-1}) than that expected for the two non-interacting phases (75 Am^2 kg^{-1}), the remanence is unchanged, while H_C is lower (103 vs. 239 kA m^{-1}). This experimental evidence suggests that, with a standard annealing approach, the magnetic coupling between the two phases took place only at very high temperature (1100 °C). The occurrence of the coupling at 1100 °C only is further supported by the analysis of the first derivative of the demagnetization branches (insets of figure 10): the first derivatives of samples annealed up to 900 °C display two peaks, one at very low
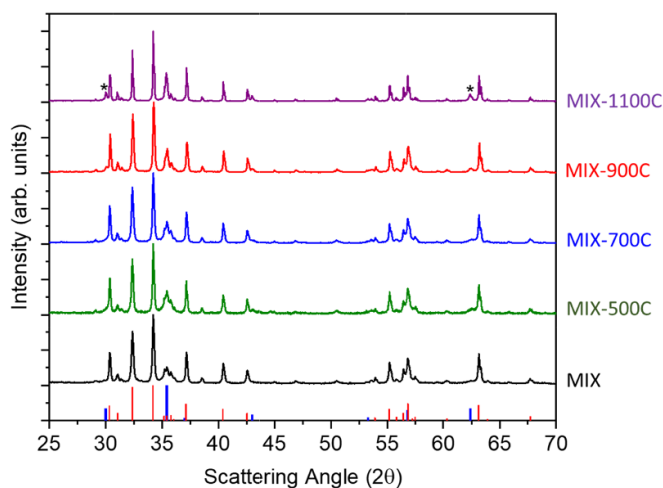
Figure 7. XRD patterns of the MIX powders annealed at different temperatures (500 °C, 700 °C, 900 °C and 1100 °C) for 2 h. The blue and red references are the ZFO and SFO ones (JCPDF: 88-0316 and 33-1340, respectively).

Table 3. *a* and *c*: lattice parameters obtained from XRD data analysis (errors on the least significant digit are reported in brackets) for both SFO and ZFO phases.

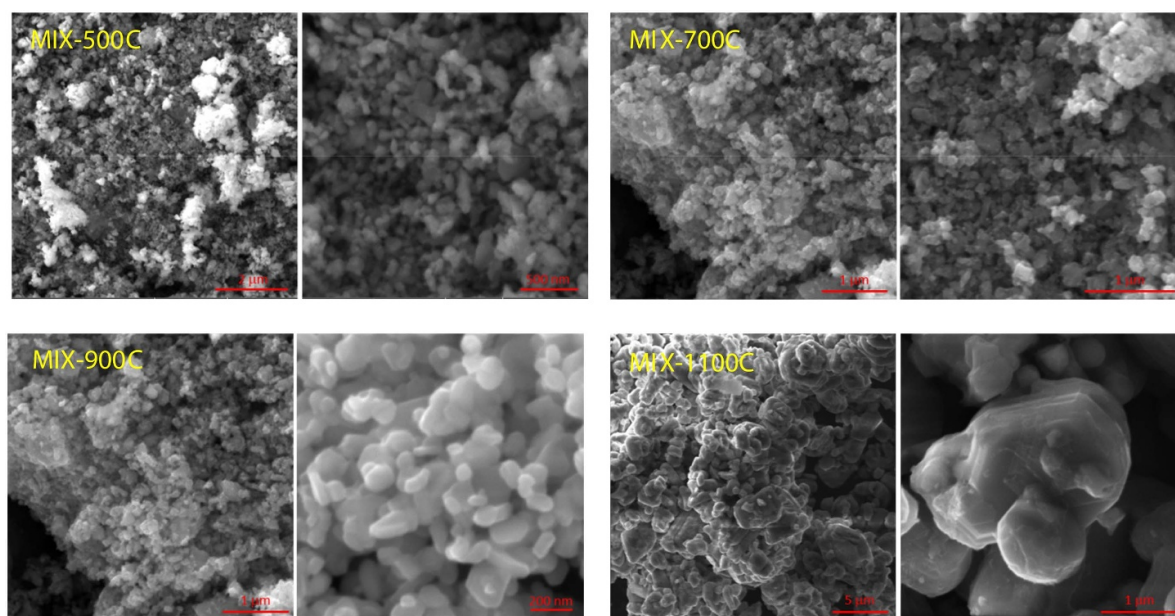| Sample	SFO lattice parameters		ZFO lattice parameter	SFO d_{XRD}	ZFO d_{XRD}
	a (nm)	*c* (nm)	*a* (nm)	(nm)	(nm)
MIX	0.5885(1)	2.3045(1)	0.8413(1)	100(10)	10(1)
MIX-500 °C	0.5884(1)	2.3035(1)	0.8410(1)	90(20)	10(1)
MIX-700 °C	0.5884(1)	2.3035(1)	0.8409(1)	90(15)	12(2)
MIX-900 °C	0.5880(1)	2.3031(2)	0.8411(1)	140(20)	35(5)
MIX-1100 °C	0.5881(1)	2.3024(2)	0.8410(1)	345(40)	50(10)

Figure 8. SEM images of the MIX-500 °C, MIX-700 °C, MIX-900 °C and MIX-1100 °C.

field (ca. 0.80 kA m^{-1}) and one at ca. ±400 kA m^{-1}, corresponding to the reversal of the two independent phases; in the sample annealed at 1100 °C a single reversal process is instead observed at 119 kA m^{-1}. The drastic change of the reversal process mechanism is related to the grain growth of the two phases and the activation of a magnetic coupling regime.
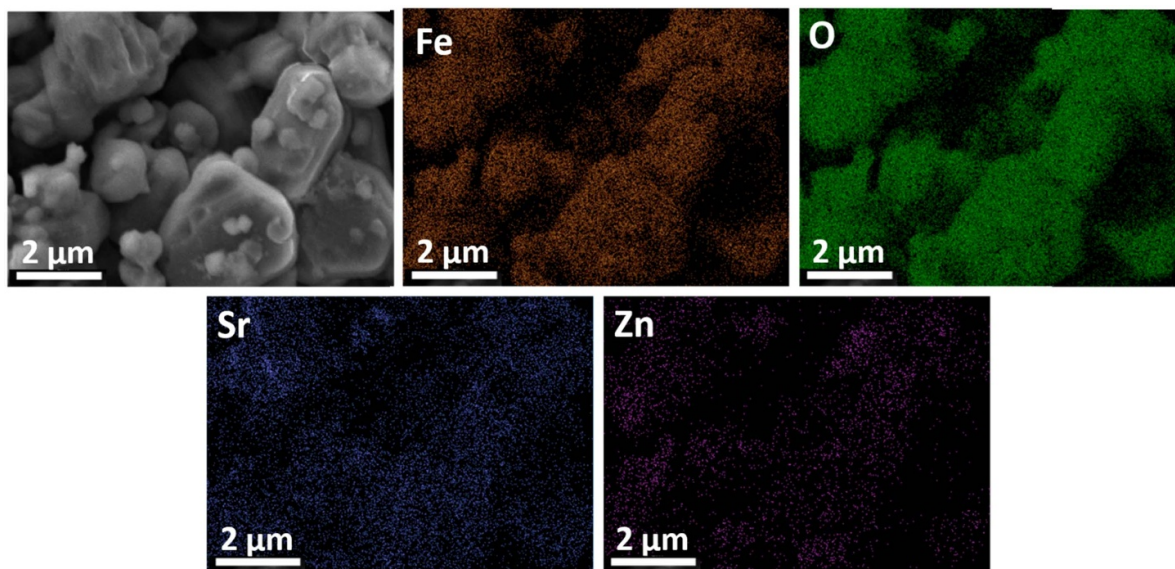
J. Phys. D: Appl. Phys. **54** (2021) 134003

M Petrecca *et al*

Figure 9. EDX mapping of MIX-1100 °C. Orange refers to Fe L$_{2,3}$, green to O K, blue to Sr L$_{2,3}$ and magenta to Zn L$_{2,3}$ edges.
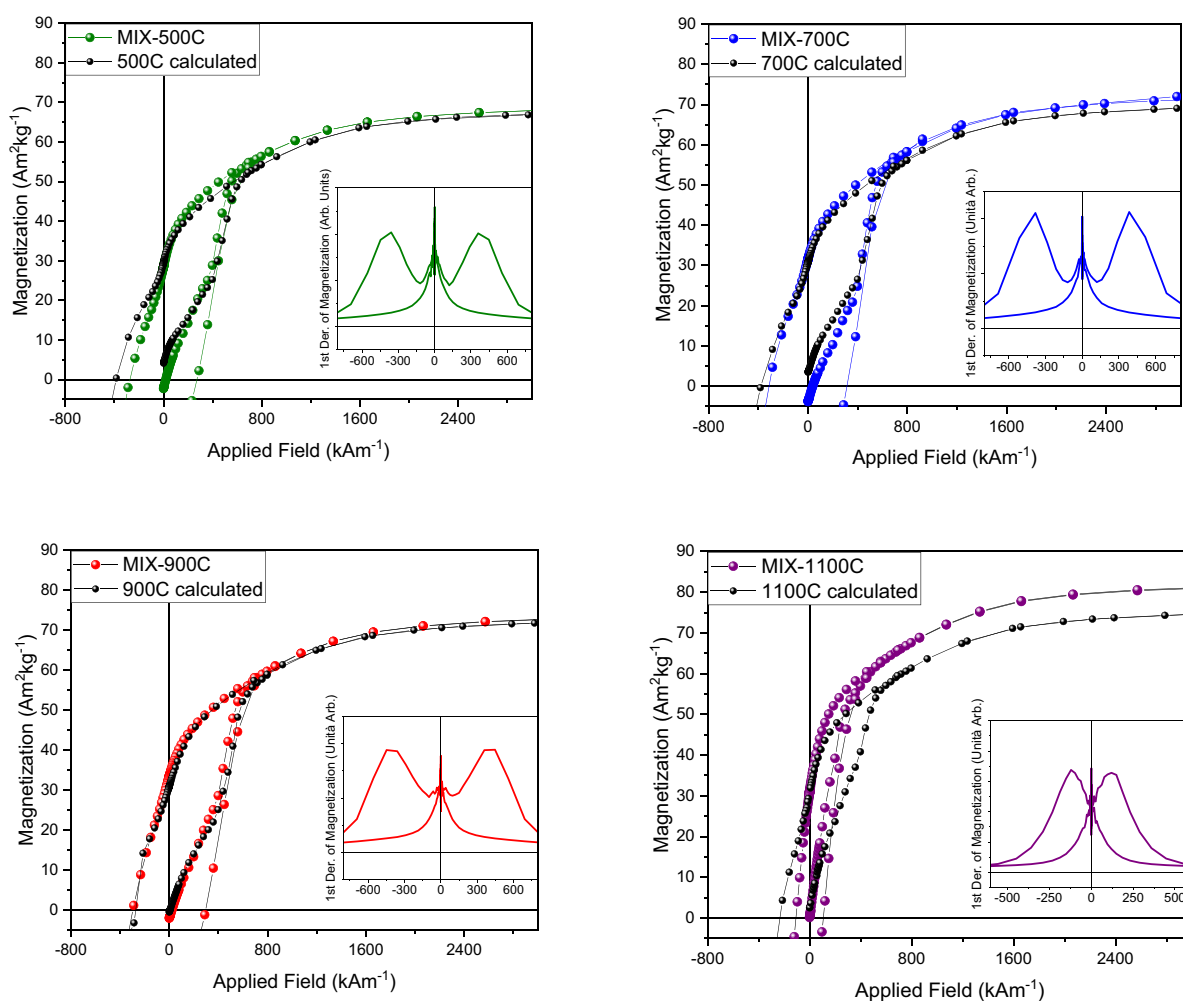

Figure 10. First magnetization curves and hysteresis loops (colored dots and lines) recorded at 300 K of the samples annealed at 500 °C (a), 700 °C (b), 900 °C (c) and 1100 °C (d) compared with the calculated ones (black symbols). Calculated curves were obtained by summing, in the ratio 90:10, the magnetization separately measured on the hard and soft powders, annealed at the target temperature.

Below 1100 °C, both phases keep their original size, and coupling is operative only through dipolar interaction, which apparently is not strong enough to lead to a single reversal process. The observation of the two independent crystal structures with an unchanged composition at 1100 °C excludes the possibility that a single crystallographic phase has been formed by the annealing. Moreover, the particle sizes of the SFO and ZFO particles, although larger, remain below the single-domain size, where incoherent reversal processes might be operative and favor the softening of the coercivity, without affecting the magnetic coupling regime. We can reasonably suppose that the observed coupling arises from a strong exchange interaction between the two metal oxides, which originates from the inclusion of smaller soft particles during the coalescence of SFO grains. However, despite successfully providing an exchange coupled system with a nanometric texture, this is not enough to improve the performance of the final hard/soft composite ($BH_{max} = 6.8$ kJ m^{-3}) with respect to the starting SFO ($BH_{max} = 7.9$ kJ m^{-3}), because of its softer behavior. This can also possibly be ascribed to the size of the soft phase, which although nanometric is still too large for effective coupling. A more systematic study of the coupling conditions (powder size, soft/hard percentage adjustment, etc), possibly combined with a more sophisticated sintering procedure (spark plasma or high pressure), is thus needed to make the materials we individually optimized useful for PM applications.

4. Conclusions

In this work, we report an investigation aimed at optimizing the properties of hard and soft building blocks to produce an exchange spring PM. The synthesized nanometric SFO had saturation magnetization and remanence close to the bulk values, and a very high coercive field (525 kA m^{-1}). The stability of this material as a function of annealing temperature was confirmed in the range 500–1100 °C, even if H_C strongly decreased at the highest investigated temperature. The structural and chemical stability of the soft $Zn_xFe_{3-x}O_4$ particles as a function of annealing temperature was also demonstrated in the range 500–1100 °C. In order to maximize the magnetization of the soft phase, a systematic investigation of the dependence of the magnetic properties on the Zn content was carried out. We found the highest saturation magnetization value for $x = 0.3$ (106 Am^2 kg^{-1}) after powder annealing at 1100 °C.

A preliminary study to produce an exchange-coupled composite was also carried out through a standard annealing procedure up to 1100 °C. The two crystallographic phases were found to be stable up to the highest investigated temperature. The size of the grains remained constant up to 900 °C, before a sintering process started leading to the growth of polycrystalline SFO grains with size in the range corresponding to the maximum coercive field. The growth of the ZFO is instead limited so that the particles preserve the nanometric size. The recorded magnetic properties indicated the coupling occurs only when the nanopowders are annealed at the highest temperature, probably due to the exchange coupling arising from the inclusion of ZFO MNPs in the growing SFO grains. However, the softening of the final product with respect to the starting SFO, at present, makes this kind of composite unsuited for realizing PMs, suggesting that further work needs to be done. In particular, a careful investigation on different coupling procedures, such as spark plasma sintering or high-pressure-field-assisted sintering approaches, could lead to a higher BH_{max}.

ORCID iDs

Michele Petrecca ⓘ https://orcid.org/0000-0002-4895-0254
Beatrice Muzzi ⓘ https://orcid.org/0000-0001-9151-7723
Martin Albino ⓘ https://orcid.org/0000-0001-7438-0833
Davide Peddis ⓘ https://orcid.org/0000-0003-0810-8860
César de Julián Fernández ⓘ https://orcid.org/0000-0002-6671-2743
Claudia Innocenti ⓘ https://orcid.org/0000-0003-3705-4283
Claudio Sangregorio ⓘ https://orcid.org/0000-0002-2655-3901

References

[1] Gutfleisch O, Willard M A, Brück E, Chen C H, Sankar S G and Liu J P 2011 Magnetic materials and devices for the 21st century: stronger, lighter, and more energy efficient *Adv. Mater.* **23** 821–42
[2] Strnat K J 1990 Modern permanent magnets for applications in electro-technology *Proc. IEEE* **78** 923–46
[3] Jimenez-Villacorta F and Lewis L H 2014 Advanced permanent magnetic materials *Nanomagnetism* ed J M Gonzalez Estevez (Spain: One Central Press) pp 160–89
[4] Coey J M D 2020 Perspective and prospects for rare earth permanent magnets *Engineering* **6** 119–31
[5] Anon (available at: https://price.metal.com/Rare-Earth)
[6] Eur. Comm. 2017 Critical raw materials ec.europa.eu › regdoc › rep › 2017
[7] Kneller E F and Hawig R 1991 The exchange-spring magnet: a new material principle for permanent magnets *IEEE Trans. Magn.* **27** 3560–88
[8] Fullerton E E, Jiang J and Bader S 1999 Hard/soft magnetic heterostructures: model exchange-spring magnets *J. Magn. Magn. Mater.* **200** 392–404
[9] Asti G, Ghidini M, Pellicelli R, Pernechele C, Solzi M, Albertini F, Casoli F, Fabbrici S and Pareti L 2006 Magnetic phase diagram and demagnetization processes in perpendicular exchange-spring multilayers *Phys. Rev.* B **73** 094406

J. Phys. D: Appl. Phys. **54** (2021) 134003

M Petrecca *et al*

[10] Ghidini M, Asti G, Pellicelli R, Pernechele C and Solzi M 2007 Hard–soft composite magnets *J. Magn. Magn. Mater.* **316** 159–65

[11] Quesada A *et al* 2016 Energy product enhancement in imperfectly exchange-coupled nanocomposite magnets *Adv. Electron. Mater.* **2** 1500365

[12] Muzzi B *et al* 2020 Unraveling the mechanism of the one-pot synthesis of exchange coupled Co-based nano-heterostructures with a high energy product *Nanoscale* **12** 14076–86

[13] Torkian S and Ghasemi A 2019 Energy product enhancement in sufficiently exchange-coupled nanocomposite ferrites *J. Magn. Magn. Mater.* **469** 119–27

[14] Nandwana V, Chaubey G S, Yano K, Rong C and Liu J P 2009 Bimagnetic nanoparticles with enhanced exchange coupling and energy products *J. Appl. Phys.* **105** 014303

[15] Liu B W, Zhang Z, Liu J and Chen L 2002 Exchange coupling and remanence enhancement in nanocomposite multilayer magnets *Adv. Mater.* **14** 1833–4

[16] Sakuma N, Ohshima T, Shoji T, Suzuki Y, Sato R, Wachi A, Kato A, Kawai Y, Manabe A and Teranishi T 2011 Exchange coupling interaction in L 1 0-FePd/α-Fe nanocomposite magnets with large maximum energy products *ACS Nano* **5** 2806–14

[17] Gao R W *et al* 2003 Exchange-coupling interaction, effective anisotropy and coercivity in nanocomposite permanent materials *J. Appl. Phys.* **94** 664–8

[18] Skomski R and Coey J M D 1993 Giant energy product in nanostructured two-phase magnets *Phys. Rev.* B **48** 15812–6

[19] Pan L, Cao D, Jing P, Wang J and Liu Q 2015 A novel method to fabricate $CoFe_2O_4$/$SrFe_{12}O_{19}$ composite ferrite nanofibers with enhanced exchange coupling effect *Nanoscale Res. Lett.* **10** 131

[20] Volodchenkov A D, Kodera Y and Garay J E 2016 Synthesis of strontium ferrite/iron oxide exchange coupled nano-powders with improved energy product for rare earth free permanent magnet applications *J. Mater. Chem.* C **4** 5593–601

[21] Tavakolinia F, Yousefi M, Afghahi S, Baghshahi S and Samadi S 2018 Synthesis of novel hard/soft ferrite composites particles with improved magnetic properties and exchange coupling *Process. Appl. Ceram.* **12** 248–56

[22] Xia A, Ren S, Lin J, Ma Y, Xu C, Li J, Jin C and Liu X 2015 Magnetic properties of sintered $SrFe_{12}O_{19}$–$CoFe_2O_4$ nanocomposites with exchange coupling *J. Alloys Compd.* **653** 108–16

[23] Nga T T V, Thi Lan N, Thanh Loan T and Ha H 2019 Structure and magnetic properties of $SrFe_{12}O_{19}$/$CoFe_2O_4$ nanocomposite ferrite *VNU J. Sci. Math. Phys.* **35** 1289–93

[24] Dong J, Zhang Y, Zhang X, Liu Q and Wang J 2014 Improved magnetic properties of $SrFe_{12}O_{19}$/FeCo core–shell nanofibers by hard/soft magnetic exchange-coupling effect *Mater. Lett.* **120** 9–12

[25] Li D, Wang F, Xia A, Zhang L, Li T, Jin C and Liu X 2016 A facile way to realize exchange coupling interaction in hard/soft magnetic composites *J. Magn. Magn. Mater.* **417** 355–8

[26] Jenuš P, Topole M, McGuiness P, Granados-Miralles C, Stingaciu M, Christensen M, Kobe S and Žužek Rožman K 2016 Ferrite-based exchange-coupled hard–soft magnets fabricated by spark plasma sintering ed A Belik *J. Am. Ceram. Soc.* **99** 1927–34

[27] Song F, Shen X, Liu M and Xiang J 2011 Preparation and magnetic properties of $SrFe_{12}O_{19}$/$Ni_{0.5}Zn_{0.5}Fe_2O_4$ nanocomposite ferrite microfibers via sol–gel process *Mater. Chem. Phys.* **126** 791–6

[28] Hölscher J, Petrecca M, Albino M, Garbus P G, Saura-Múzquiz M, Sangregorio C and Christensen M 2020 Magnetic property enhancement of spinel Mn–Zn ferrite through atomic structure control *Inorg. Chem.* **59** 11184–92

[29] Šepelák V, Baabe D, Mienert D, Schultze D, Krumeich F, Litterst F J and Becker K D 2003 Evolution of structure and magnetic properties with annealing temperature in nanoscale high-energy-milled nickel ferrite *J. Magn. Magn. Mater.* **257** 377–86

[30] Tung L, Kolesnichenko V, Caruntu G, Caruntu D, Remond Y, Golub V, O'Connor C and Spinu L 2002 Annealing effects on the magnetic properties of nanocrystalline zinc ferrite *Physica* B **319** 116–21

[31] Ai L and Jiang J 2010 Influence of annealing temperature on the formation, microstructure and magnetic properties of spinel nanocrystalline cobalt ferrites *Curr. Appl. Phys.* **10** 284–8

[32] Hu P, Yang H, Pan D, Wang H, Tian J, Zhang S, Wang X and Volinsky A A 2010 Heat treatment effects on microstructure and magnetic properties of Mn–Zn ferrite powders *J. Magn. Magn. Mater.* **322** 173–7

[33] Kiani E, Rozatian A S H and Yousefi M H 2013 Synthesis and characterization of $SrFe_{12}O_{19}$ nanoparticles produced by a low-temperature solid-state reaction method *J. Mater. Sci., Mater. Electron.* **24** 2485–92

[34] Smit J and Wijn H P J 1959 Ferrites Philips Technical Lybrary (Eindhoven: N V Philips' Gloeilampenfabrieken) pp 384

[35] Raju K, Venkataiah G and Yoon D H 2014 Effect of Zn substitution on the structural and magnetic properties of Ni–Co ferrites *Ceram. Int.* **40** 9337–44

[36] Yafet Y and Kittel C 1952 Antiferromagnetic arrangements in ferrites *Phys. Rev.* **87** 290–4

[37] Petitt G A and Forester D W 1971 Mössbauer study of cobalt–zinc ferrites *Phys. Rev.* B **4** 3912–23

[38] Pawley G S 1981 Unit-cell refinement from powder diffraction scans *J. Appl. Crystallogr.* **14** 357–61

[39] Jang J T, Nah H, Lee J H, Moon S H, Kim M G and Cheon J 2009 Critical enhancements of MRI contrast and hyperthermic effects by dopant-controlled magnetic nanoparticles *Angew. Chem., Int. Ed.* **48** 1234–8

[40] O'Neill H S C and Navrotsky A 1984 Cation distributions and thermodynamic properties of binary spinel solid solutions *Am. Mineral.* **69** 733–53

[41] Cullity B D and Graham C D 2011 *Introduction to Magnetic Materials* (Wiley-IEEE Press)

[42] Modaresi N, Afzalzadeh R, Aslibeiki B, Kameli P, Ghotbi Varzaneh A, Orue I and Chernenko V A 2019 Magnetic properties of $Zn_xFe_{3−x}O_4$ nanoparticles: a competition between the effects of size and Zn doping level *J. Magn. Magn. Mater.* **482** 206–18

[43] Liu J, Bin Y and Matsuo M 2012 Magnetic behavior of Zn-doped Fe_3O_4 nanoparticles estimated in terms of crystal domain size *J. Phys. Chem.* C **116** 134–43

[44] Albino M *et al* 2019 Role of Zn^{2+} substitution on the magnetic, hyperthermic, and relaxometric properties of cobalt ferrite nanoparticles *J. Phys. Chem.* C **123** 6148–57

[45] Mallesh S and Srinivas V 2019 A comprehensive study on thermal stability and magnetic properties of MnZn-ferrite nanoparticles *J. Magn. Magn. Mater.* **475** 290–303

[46] Thakur S, Katyal S C, Gupta A, Reddy V R and Singh M 2009 Room temperature ferromagnetic ordering in indium substituted nano-nickel–zinc ferrite *J. Appl. Phys.* **105** 07A521

[47] Hamdeh H H, Ho J C, Oliver S A, Willey R J, Oliveri G and Busca G 1997 Magnetic properties of partially-inverted zinc ferrite aerogel powders *J. Appl. Phys.* **81** 1851–7

[48] Yang Y, Liu X, Yang Y, Xiao W, Li Z, Xue D, Li F and Ding J 2013 Synthesis of nonstoichiometric zinc ferrite nanoparticles with extraordinary room temperature

magnetism and their diverse applications *J. Mater. Chem.* C **1** 2875

[49] Ramírez A E, Solarte N J, Singh L H, Coaquira J A H and Gaona J S 2017 Investigation of the magnetic properties of SrFe$_{12}$O$_{19}$ synthesized by the Pechini and combustion methods *J. Magn. Magn. Mater.* **438** 100–6

[50] Kojima H 1982 Fundamental properties of hexagonal ferrites with magnetoplumbite structure *Handbook of Ferromagnetic Materials* Wohlfarth E P (Amsterdam: North Holland) vol 3 ch 5 pp 305–91

[51] Sánchez-De Jesús F, Bolarín-Miró A M, Cortés-Escobedo C A, Valenzuela R and Ammar S 2014 Mechanosynthesis, crystal structure and magnetic characterization of M-type SrFe$_{12}$O$_{19}$ *Ceram. Int.* **40** 4033–8

[52] Kostishyn V G, Panina L V, Kozhitov L V, Timofeev A V and Kovalev A N 2015 Synthesis and multiferroic properties of M-type SrFe$_{12}$O$_{19}$ hexaferrite ceramics *J. Alloys Compd.* **645** 297–300

[53] Pullar R C 2012 Hexagonal ferrites: a review of the synthesis, properties and applications of hexaferrite ceramics *Prog. Mater. Sci.* **57** 1191–334

[54] Guo Z-B, Ding W-P, Zhong W, Zhang J-R and Du Y-W 1997 Preparation and magnetic properties of SrFe$_{12}$O$_{19}$ particles prepared by the salt-melt method *J. Magn. Magn. Mater.* **175** 333–6

[55] Zi Z F, Sun Y P, Zhu X B, Yang Z R, Dai J M and Song W H 2008 Structural and magnetic properties of SrFe$_{12}$O$_{19}$ hexaferrite synthesized by a modified chemical co-precipitation method *J. Magn. Magn. Mater.* **320** 2746–51

[56] Verma A, Pandey O P and Sharma P 2010 ChemInform abstract: strontium ferrite permanent magnet—an overview *ChemInform* **32**

[57] Hirayama T, Ru Q, Tanji T and Tonomura A 1993 Observation of magnetic-domain states of barium ferrite particles by electron holography *Appl. Phys. Lett.* **63** 418–20